Spontaneous spin polarization in geometrically constricted metal nanowires

R. Cortes-Huerto and P. Ballone
Atomistic Simulation Centre, Queen's University Belfast, Belfast BT7 1NN, United Kingdom
(Received 30 September 2009; revised manuscript received 8 November 2009; published 29 December 2009)

The electronic structure of thin conducting wires with a narrow geometric constriction has been determined by density-functional theory computations in the local spin density approximation. Spontaneous spin polarization arises in nominally paramagnetic wires at sufficiently low density ($r_s \geq 15$). Real-space spin-polarization maps show a fascinating variety of magnetic structures pinned at the constriction. The frequency-dependent conductivity is different for the spin-up and spin-down channels and significantly lower than in wires of identically vanishing spin polarization.

DOI: 10.1103/PhysRevB.80.233304 PACS number(s): 73.21.Hb, 72.25.−b, 73.22.Gk, 73.63.Nm

Conducting wires of nanometric diameter are emerging as a powerful paradigm for the interplay of dimensionality, electron correlation, and dynamics. Luttinger liquid phases,[1] spontaneous spin polarization,[2] and Wigner crystallization[3] are among the most intriguing phenomena that have been predicted and increasingly revealed in nanowires.

Reduced dimensionality, in particular, is reflected in the conductivity quantization[4] of nanometric wires in units of $2e^2/h$. Integer quantization is violated by the so-called 0.7 anomaly[2] if the translational symmetry along the wire is broken by a geometric constriction, applied by stretching a metal wire to a near-breaking condition,[5] or by electrostatic patterning of doped semiconducting nanostructures.[2,6] The 0.7 anomaly is generally attributed to spontaneous spin polarization at the constriction of an otherwise paramagnetic conductor.[2]

It has been known for some time that density-functional theory–local spin density (DFT-LSD) does reproduce the spontaneous spin polarization of nanowires[8,9] of sufficiently low electron density.[7–9] Most studies, however, adopted simplifying assumptions (such as axial symmetry) to reduce the complexity of the computation. Large-scale simulations of a three-dimensional (3D) model of constricted metal wires, free of symmetry restrictions, reveal complex configurations of unpaired spins pinned at the geometric constriction. Polarization is reflected in the asymmetry of conductivity in the spin-up and spin-down channels and in the decrease in the total conductivity with respect to the case of paramagnetic wires. Although our approach is not expected to quantitatively reproduce neither integer quantization nor the 0.7 anomaly, it still provides a diagnostic signal of impending transitions in the ground state.

We adopt the most idealized picture of conducting wires based on the jellium model. The system consists of $N=N_{up}+N_{dn}$ electrons neutralized by a cylindrical distribution of positive charge, where N_{up} and N_{dn} are the number of spin-up and spin-down electrons, respectively. The positive charge has constant density ρ_+ within the cylinder and zero outside. In what follows, the ρ_+ density is expressed in terms of the Wigner-Seitz radius[10] $r_s=(3/4\pi\rho_+)^{1/3}$. The axis of the cylinder is aligned along z; the wire diameter $2R_c$ and length L_z satisfy the neutrality condition $\rho_+\pi R_c^2 L_z=(N_{up}+N_{dn})$. The indentation is obtained by removing a solid of revolution generated by rotating a parabolic segment around the z axis as shown in Fig. 1. The system is replicated in 3D with the same periodicity $L(=L_z)$ in all directions, and the total energy $E[\rho]$ is expressed by the local spin density approximation of density-functional theory[11] using the Perdew-Zunger interpolation[12] for the exchange-correlation energy.

The sampling of the one-dimensional Brillouin zone is restricted to the Γ point only. We verified by explicit computations at $r_s=3$ that the difference in eigenvalues at the Γ point and at the zone boundary is negligible and, thus, restricting our sampling to the Γ point does not affect our results. Dispersion is less important at lower densities, especially when progressive localization prevents the interaction of electrons with periodic images in neighboring simulation cells. Moreover, the Γ-point approximation might be more relevant for experimental nanowires, whose aspect ratio L_z/R_c is never very high.

Comparison of LSD results with quantum Monte Carlo data show that LSD is remarkably accurate for inhomogeneous jellium systems.[13] Semilocal approaches such as generalized gradient approximations[14] provide results very similar to those of LSD for jelliumlike systems. Resorting to local and semilocal DFT approximations might exclude *a priori* the observation of exotic phases at low electron density.

Kohn-Sham (KS) orbitals are expanded in plane waves of wave vectors $\mathbf{G}$ compatible with the 3D system periodicity, i.e., belonging to the reciprocal lattice of the periodic repetition of simulation cells:[7]

$$\psi_j(\mathbf{r}) = \sum_{\mathbf{G}} c_{\mathbf{G}}^{(j)} e^{i\mathbf{G}\mathbf{r}}. \quad (1)$$

The sum extends over all reciprocal lattice vectors such that $|\mathbf{G}| \leq G_{cut}$. The ground-state structure is determined by direct minimization of $E[\rho]$ with respect to the coefficients $\{c_{\mathbf{G}}^{(j)}\}$, and empty states are computed by the minimization strategy of Ref. 7.

The kinetic energy cutoff for the plane-wave expansion has been set to $E_{cut}=20/r_s^2$. All samples are globally spin compensated, having $N_{up}=N_{dn}=115$, but spin polarization may appear locally as a way to decrease energy, driven by exchange.

The frequency-dependent conductivity along z is computed using the Greenwood-Kirkwood expression[11]

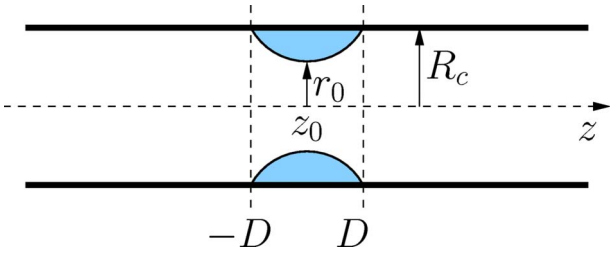

FIG. 1. (Color online) Schematic of the positive charge distribution.

$$\sigma(\omega) = \frac{ie^2}{m^2\Omega}\sum_{n,n'}\sum_{\mathbf{k},\mathbf{k}'}\frac{1}{\omega}\frac{f(\epsilon^{n'}_{\mathbf{k}'}) - f(\epsilon^{n}_{\mathbf{k}})}{(\epsilon^{n'}_{\mathbf{k}'} - \epsilon^{n}_{\mathbf{k}}) - \hbar\omega - i\hbar\eta}|\langle\psi^{n'}_{\mathbf{k}'}| - i\hbar\nabla_{\mathbf{r}}|\psi^{n}_{\mathbf{k}}\rangle|^2, \quad (2)$$

where $f(\epsilon)$ are electron occupation numbers, the ϵ's are Kohn-Sham eigenvalues, and both $\mathbf{k}$ and $\mathbf{k}'$ coincide with the Γ point. To be precise, the $\sigma(\omega)$ defined above is the zz component of the 3×3 conductivity tensor, whose other elements identically vanish in this case.

In what follows, we focus primarily on the low density ($r_s > 10$) regime that is achieved in lightly doped semiconductor nanostructures and in conducting polymers. Although we write our equations for the simplest case of bare electrons in an external potential, these can be adapted to the case of electrons and holes in a dielectric medium by rescaling the free carrier mass and introducing a dielectric constant. Our computational approach can easily be adapted to other, less symmetric geometries used in experiments. The results, however, are expected to be qualitatively the same of the cylindrical case.

We emphasize again that Eq. (2), based on an independent electron picture, is not expected to capture genuine many-body effects such as the 0.7 anomaly. Nevertheless, the destabilization of the paramagnetic ground state and the role of the indentation manifest themselves in the spontaneous polarization of spins that starts at the constriction. On the other hand, the replacement of the atomic structure with an idealized pseudopotential (jellium) is likely to be unimportant at low density ($r_s > 10$), since the orbitals we compute are in fact simple approximations to quasiparticle wave functions extending over many atoms, and whose energy scale (a few meV) is too low to cause any significant change in the atomic structure.

Similar computations for cylindrical wires[7] (no constriction) predict spontaneous spin polarization and charge localization to take place continuously and nearly simultaneously with decreasing density, as the energy of low amplitude inhomogeneities decreases toward zero. According to DFT-LSD, local spin polarization is well established at $r_s=25$ and charge localization at $r_s=30$. For $r_s \geq 40$ the ground state of cylindrical nanowires turns out to be fully spin polarized.

We start from a cylindrical distribution of positive charge of $R_c=3.162r_s$, $L_z=32r_s$, neutralizing 240 electrons. The indentation is introduced by removing ten electrons together with the corresponding amount of positive charge. The constriction parameters are $r_0=0.37R_c$ and $D=0.34R_c=1.04r_s$ (see Fig. 1). Then, the system consists of $N=230$ electrons, the minimum cross section is equal to 14% of the original cylindrical one, and the linear size of the neck is comparable to the average separation between two electrons, i.e., $\sim 2r_s$. The density range from $r_s=3$ to $r_s=70$ has been explored.

For the $r_s=3$ case, i.e., well within the density range of simple metals, inspection of the spin-polarization density $m(\mathbf{r})=\rho_{up}(\mathbf{r})-\rho_{dn}(\mathbf{r})$ shows that spin compensation, globally enforced by our choice $N_{up}=N_{dn}$, is valid also locally, apart from small spin fluctuations of less than 1% ρ_+, primarily due to shell effects already described in Ref. 15. The spin-up and spin-down density of states (DOS) virtually coincide. Differences between the DOS of wires with and without constriction are minor and reflect again shell effects. As expected, no gap separates occupied and unoccupied states.

At first, the picture provided by the computation remains qualitatively the same with decreasing density, even though the amplitude of spin-polarization waves tends to increase slowly but fairly monotonically with increasing r_s. At $r_s=15$, the slow increase in $|m(\mathbf{r})|$ has given rise to recognizable magnetization structures at a background density which is somewhat higher than the one ($r_s \sim 25$; Ref. 7) at which spontaneous spin polarization appears in wires of constant cross section. In the constricted wire at $r_s=15$, the spin-polarization density is distributed over the entire length of the simulated sample. However, it is also apparently in registry with the indentation giving rise to symmetric patterns on the two sides of the constriction.

The onset of the spin polarization at $r_s=15$ is marked by increasing difficulties in the energy minimization due to the appearance of distinct, nearly degenerate local minima in the dependence of $E[\rho]$ on the $\{c^{(j)}_{\mathbf{G}}\}$'s. Multiple minima manifest themselves especially in the difficulty of separating states above and below the Fermi energy as required to consistently assign occupation numbers. Convergence in the occupation numbers is achieved in all cases by combining minimization with subdiagonalization of the Hamiltonian on a restricted basis made of occupied and empty states as determined by the energy minimization.

Spin magnetization structures, first identified at $r_s=15$, are fully developed at $r_s=20$. Also in this case, the nonvanishing spin density is in registry with the background indentation, and, again, it extends over the entire length of the wire [see Fig. 2(a)]. Starting from $r_s=20$, however, a remarkable and complex spin-polarization pattern is located at or in close proximity of the constriction. The precise shape of this structure sensitively depends on r_s. This is emphasized by the results for $r_s=30$ [see Fig. 2(b)], showing a sizable degree of spin and charge localization, apparently enhanced in close proximity of the indentation. To fairly high accuracy, each of the charge/spin blobs seen in Fig. 2(b) corresponds to one electron.

Because of the global spin compensation, and in the absence of external perturbations coupled to spin, the role of the *up* and *dn* spin components is completely symmetric, and for each sample the sign of local magnetization is determined only by the (random) starting point. The picture seen in the density and spin-polarization isosurfaces at $r_s=30$ remains qualitatively the same with increasing r_s up to $r_s=70$. How-

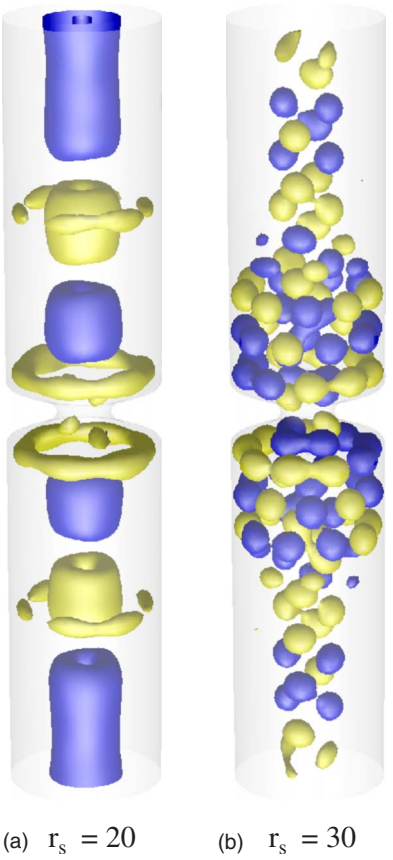

FIG. 2. (Color online) Isosurfaces of the electron magnetization $m(\mathbf{r})$ for the $r_s=20$ [panel (a) blue (dark) surface: $+0.2\rho_+$; yellow (light) surface: $-0.2\rho_+$] and $r_s=30$ [panel (b) blue (dark) surface: $+1.2\rho_+$; yellow (light) surface: $-1.2\rho_+$] nanoconstricted wires. The light gray surface represents the background.

ever, localization becomes stronger, and the spin asymmetry across the indentation becomes comparably less important, with exchange progressively losing ground to correlation.

Spin polarization and charge localization at low density are basic features in the homogeneous electron gas phase diagram. In this respect, the results for the constricted nanowire, therefore, are not particularly surprising, even though the density at which they first occur is somewhat higher than in the unconstricted case. Far more important for our discussion is the apparent relation of polarization and localization with the geometric constriction, which is highlighted in Figs. 2(a) and 2(b).

The remarkable features seen in the density and spin-polarization distributions are only mildly reflected in the spin-resolved density of states at least down to $r_s=30$. The spin-up and spin-down density of states are already different for $r_s \geq 15$, but differences are not large, as can be seen in Fig. 3. Moreover, at $15 \leq r_s \leq 30$ the Fermi level sits in a local minimum of the DOS (pseudogap), but no real gap opens up unless we release the $N_{up}=N_{dn}$ constraint. In we define separate Fermi energies for spin-up and spin-down electrons, the difference in the two values is vanishingly small when we impose $N_{up}=N_{dn}$, and it has been neglected in Fig. 3. In the case of cylindrical wires, the fully unconstrained optimization (i.e., not imposing $N_{up}=N_{dn}$) at $r_s=30$

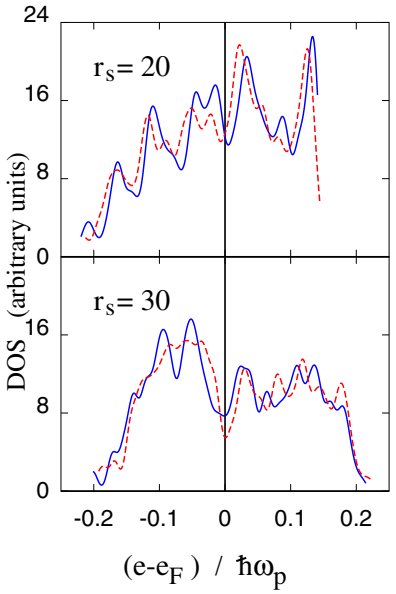

FIG. 3. (Color online) Spin-resolved density of states at $r_s=20$ and $r_s=30$. Blue full line: spin-up states; red dashed line: spin-down states.

gives a partially polarized, partially charge localized ground state whose corresponding DOS has a clear gap at E_F.

Analysis of electron localization, measured by the inverse participation ratio of individual Kohn-Sham states, shows that, as expected, the most localized states are those whose eigenvalue is close to the Fermi energy. However, no single KS state, either occupied or empty, is strictly localized at the constriction, and several states contribute to the projected DOS at the indentation.

The breaking of the spin symmetry is more apparently reflected in the electron conductivity. At $r_s=3$, the energy-dependent conductivity $\sigma(\omega)$ computed using Eq. (2) is fully symmetric in the spin-up and spin-down channels, it decays nearly monotonically with increasing ω, and vanishes for $\hbar\omega > 0.5$ eV (Fig. 4). At lower density, our computations provide clear evidence of the loss of spin symmetry in the conductivity resulting from the partial spin polarization (see Fig. 4). The asymmetry arises at $r_s \sim 15$ and persists down to the lowest density considered in our study ($r_s=70$). However, the relative asymmetry decreases somewhat below the $r_s=30$ density, when localization sets in, reducing conductivity in both spin channels.

As a comparison, $\sigma(\omega)$ is restricted to a delta function at $\omega=0$ for the cylindrical case (no indentation) at all densities such that $\rho(\mathbf{r})$ is translationally invariant. On the other hand, even in wires without indentation, the Greenwood-Kirkwood expression (2) for $\sigma(\omega)$ predicts weak contributions at non-vanishing frequency at densities ($20 \leq r_s \leq 30$) such that the ground state is partially spin polarized and charge localized. In these cases, a weak asymmetry between the two spin channels of the conductivity is also observed quantitatively much less important than in constricted wires.

Computations carried out within the spin-restricted local-density approximation, i.e., by imposing $\rho_{up}(\mathbf{r})=\rho_{dn}(\mathbf{r})$ everywhere, result in a density distribution that is less localized than the one given by the spin-unrestricted approach. As a

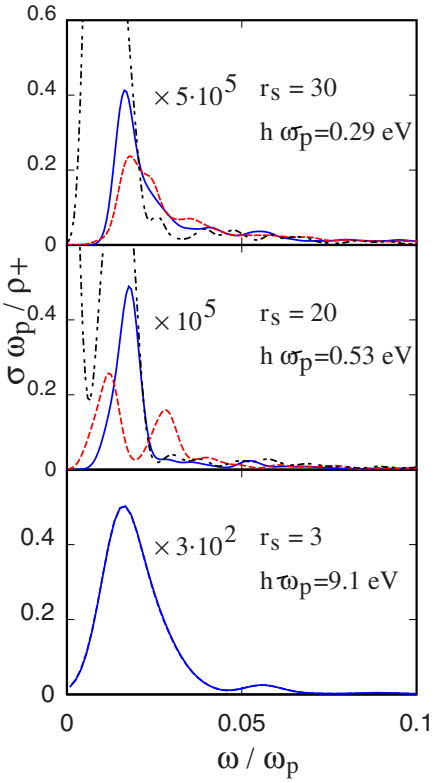

FIG. 4. (Color online) Spin-resolved conductivity at $r_s=3$, $r_s=20$, and $r_s=30$. Blue full line: spin up; red dashed line: spin down; black dash-dotted line: identically paramagnetic solution (see text).

consequence, the conductivity of the spin compensated case is higher than the sum of the spin-up and spin-down conductivities of the spin-unrestricted case. In other words, spontaneous spin polarization favors localization and decreases conductivity.

In conclusion, spin and symmetry unrestricted computations in the DFT-LSD approximation for a jellium model of constricted nanowires predict the onset of spin polarization and charge localization at $r_s \sim 15$. Maps of the spin-polarization density $m(\mathbf{r})$ at densities lower than the $r_s=15$ value display a variety of magnetic structures, whose close association with the indentation becomes increasingly apparent with decreasing density. The spin asymmetry across the indentation is reflected in the asymmetry of electric conductivity in the spin-up and spin-down channels.

The role of the geometric constriction in enhancing spin polarization and charge localization might be rationalized as follows. Both polarization and localization are opposed by kinetic energy considerations. Inhomogeneities of the external potential, however, increase the kinetic energy of all occupied states making the extra cost of polarization and/or localization less relevant.

Our results apply to nanowires obtained by electrostatic patterning of semiconducting nanostructures.[2,6] They do not describe simple metal wires at near-breaking stretching,[5] since in that case the atomic structure is expected to play a role. To bridge the two regimes, one could resort to the so-called stabilized jellium,[16] which, to some extent, restores the role of the ionic lattice.

The picture we obtain, based on an independent electron picture such as DFT-LSD, is unable to describe the 0.7 anomaly seen in experiments. However, orbitals and energies obtained by our computations provide the input for more sophisticated, many-body Hamiltonians.[9] On the other hand, our results, providing a vivid picture of complex magnetic structures at the constriction, emphasize the role of large-scale computations, unrestricted by symmetry and spin constraints. Different exchange-correlation approximations might give quantitatively different results for magnetization. The qualitative result, however, is expected to be unchanged. Generalized gradient approximations, for instance, are known to give, in most cases, nearly the same orbitals and eigenvalues (and thus magnetization) of LSDA, even though the corresponding total energies are different.

Our results provide the starting point for time-dependent DFT-LSD computations. The near degeneracy of the ground state at low density is likely to give rise to high nonlinearity in response to applied external fields.

We thank J. P. Bird for drawing our attention to this problem.

[1] J. M. Luttinger, J. Math. Phys. **4**, 1154 (1963); S. Tomonaga, Prog. Theor. Phys. **5**, 544 (1950); M. P. A. Fisher and A. Glazman, *Mesoscopic Electron Transport* (Kluwer Academic Publishers, Boston, 1997).
[2] K. J. Thomas *et al.*, Phys. Rev. Lett. **77**, 135 (1996); K. J. Thomas *et al.*, Phys. Rev. B **58**, 4846 (1998).
[3] A. Rahman and M. K. Sanyal, Phys. Rev. B **76**, 045110 (2007).
[4] B. J. van Wees *et al.*, Phys. Rev. Lett. **60**, 848 (1988).
[5] L. Kuipers and J. W. M. Frenken, Phys. Rev. Lett. **70**, 3907 (1993).
[6] Y. Yoon *et al.*, Phys. Rev. Lett. **99**, 136805 (2007); T. Morimoto *et al.*, Appl. Phys. Lett. **82**, 3952 (2003).
[7] D. Hughes and P. Ballone, Phys. Rev. B **77**, 245312 (2008).
[8] K.-F. Berggren and I. I. Yakimenko, Phys. Rev. B **66**, 085323 (2002).
[9] Y. Meir *et al.*, Phys. Rev. Lett. **89**, 196802 (2002); K. Hirose *et al.*, *ibid.* **90**, 026804 (2003).
[10] G. Giuliani and G. Vignale, *Quantum Theory of the Electron Liquid* (Cambridge University Press, Cambridge, 2005).
[11] E. Kaxiras, *Atomic and Electronic Structure of Solids* (Cambridge University Press, Cambridge, 2003).
[12] J. P. Perdew and A. Zunger, Phys. Rev. B **23**, 5048 (1981).
[13] F. Sottile and P. Ballone, Phys. Rev. B **64**, 045105 (2001).
[14] J. P. Perdew *et al.*, Phys. Rev. B **46**, 6671 (1992).
[15] N. Zabala *et al.*, Phys. Rev. Lett. **80**, 3336 (1998).
[16] J. P. Perdew *et al.*, Phys. Rev. B **42**, 11627 (1990).